ISSN 1063-7761, Journal of Experimental and Theoretical Physics, 2018, Vol. 127, No. 4, pp. 705–712. © Pleiades Publishing, Inc., 2018.
Original Russian Text © E.I. Salamatov, A.V. Taranov, E.N. Khazanov, E.V. Charnaya, E.V. Shevchenko, 2018, published in Zhurnal Eksperimental'noi i Teoreticheskoi Fiziki, 2018, Vol. 154, No. 4, pp. 826–834.

SOLIDS AND LIQUIDS

Specific Heat and Phonon Transport in Er-Containing Rare-Earth–Aluminum Garnets at Liquid-Helium Temperatures

E. I. Salamatov[a], A. V. Taranov[b,*], E. N. Khazanov[b], E. V. Charnaya[c], and E. V. Shevchenko[c]

[a] *Udmurt Federal Scientific Center, Ural Branch, Russian Academy of Sciences, Izhevsk, 426067 Russia*
[b] *Kotel'nikov Institute of Radio Engineering and Electronics, Russian Academy of Sciences, Moscow, 103907 Russia*
[c] *Department of Physics, St. Petersburg State University, St. Petersburg, 198504 Russia*
**e-mail: taranov@cplire.ru*

Received April 21, 2018

Abstract—The temperature dependences of the specific heat and the transport characteristics of thermal-frequency phonons in single crystals of the solid solutions of rare-earth aluminum garnets are studied at liquid-helium temperatures in the presence of Schottky-type low-energy excitations. The kinetic characteristics of phonons as functions of the solid solution composition are measured. The relation between the kinetic and thermophysical characteristics of the material in the solid solutions of rare-earth aluminum garnets is analyzed under conditions of a nonstationary process and the spatial inhomogeneity caused by the coordinate dependence of the state of low-energy excitations. The thermalization conditions in the nonequilibrium phonon–low-energy excitation system are estimated.

DOI: 10.1134/S1063776118090091

1. INTRODUCTION

Rare-earth aluminum garnets (REAGs) are among the widely used laser magnetization reversal. They combine the spectral-generation properties of trivalent rare-earth ions with a high mechanical strength, chemical resistance, and optical transparence over a wide spectral region [1, 2].

Apart from the optical properties, isomorphous substitution in doping and the type of rare-earth ion determine the thermal conductivity, the permittivity, and the acoustic transparence of a material [3–5]. The synthesis of microstructured polycrystalline REAG-based ceramics, the physical properties of which are not inferior to those of single crystals [6], makes it possible to create working elements for optical devices of an arbitrary aperture. Interest in studying the magnetocaloric properties of REAGs is caused by their application in low-temperature magnetic refrigerators [7].

The presence of paramagnetic rare-earth ions in the crystal lattice of REAGs solid solutions can lead to the formation of magnetically ordered phases at temperatures [8], the appearance of nontrivial magnetic-field-induced nontrivial states [9–11], and the appearance of low-energy Schottky-type excitations in the crystal lattice of REAG. These specific features can determine the phonon transport and the thermodynamic properties at liquid-helium temperatures. An analysis of the results of independent experiments on the phonon kinetics and low-temperature specific heat $c(T)$ allows one to study the nature of low-temperature vibrational states in the range $T < 4$ K [12], which is problematic for optical spectroscopy; therefore, these effects are poorly understood in most REAGs.

Thus, the investigations of the phonon kinetics and the thermodynamic properties of garnets with a partly of fully substituted diamagnetic sublattice facilitate the understanding of the optical, magnetic, and kinetic properties of such substitutional solid solutions at liquid-helium temperatures.

An analysis of the conditions of propagation of short heat pulses at liquid-helium temperatures is a separate poorly studied problem. This problem was comprehensively considered in [13] as a result of competition of the following two mechanisms: an intense elastic (isotopic) interaction and an inelastic phonon–phonon interaction caused by lattice anharmonicity. The existence of low-energy excitations in the given temperature range substantially complicates phonon transport and brings about spatial inhomogeneity, which is related to the coordinate dependence of the state of low-energy excitations.

The purpose of this work is to study the nature of low-energy excitations and their influence on the transport characteristics of phonons and the specific heat of rare-earth garnets at liquid-helium temperatures.

2. EXPERIMENTAL

An analysis of the transport of thermal weakly nonequilibrium phonons (WNPs) in the diffusion mode at liquid-helium temperatures is a rather simple and informative method to study materials with a complex structure, including substitutional REAG solid solutions [14]. The technique used here is a developed "heat" pulse method [15]. It is characterized by the fact that the excess of phonon injector temperature T_h over thermostat temperature T_0 is such that $\Delta T = T_h - T_0 \ll T_0$ upon heating by a short current pulse ($t <$ 100 ns). In other words, phonons are weakly nonequilibrium and a sample has the thermostat temperature. Using this approach, we can study the temperature dependences of phonon diffusion coefficient $D(T)$ by changing the thermostat temperature. The lattice-anharmonicity-induced inelastic phonon–phonon interactions are unlikely in relatively short samples at liquid-helium temperatures ($T_0 < 4$ K). Therefore, the efficiency of WNP scattering under these conditions is mainly determined by elastic scattering by the "mass defect" related to the substitution of rare-earth ions at the dodecahedral c lattice sites of an REAG solid solution [14]. Time t_{m0} of the arrival of the maximum WNP diffusion signal, which is unambiguously associated with the diffusion coefficient, is measured in an experiment ("planar" geometry),

$$t_{m0}(T) = L^2/2D_0(T), \quad (1)$$

where D_0 is the diffusion coefficient during inelastic scattering of WNP ($D_0 = v^2\tau_0(\omega)/3$), v is the polarization-averaged velocity of sound, and $\tau_0(\omega)$ is the time of inelastic scattering of WNP.

Phonon–phonon processes can change the distribution of WNPs by changing their effective diffusion coefficient. Only decay processes can be effective in three-phonon processes at a small number of injected phonons [13]. Diffusion length l_{ph} during the phonon lifetime with respect to the lattice-anharmonicity-induced decay is [16]

$$l_{\text{ph}}(\omega) = \sqrt{D_0(\omega)\tau_{\text{ph}}(\omega)}, \quad (2)$$

where $\tau_{\text{ph}}(\omega)$ is the time of inelastic phonon–phonon scattering with respect to spontaneous decay.

The theoretical estimation of $\tau_{\text{ph}}(\omega)$ [17], which is based on the second- and third-order elastic constants in YAG, for thermal-frequency phonons at liquid-helium temperatures and the experimental data [18] obtained at $T = 4$ K give $\tau_{\text{ph}}(\omega) = 10^{-3}$–$10^{-2}$ s, which is higher than the experimental times of detecting a WNP signal (t_{m0}) in samples of size $L < 1$ cm at the power $P = 0.01$–0.03 W/mm^2 released in a heater [19].

Therefore, in the presence of low-energy excitations of various origins, their influence on the kinetic characteristics of phonons in relatively short samples can be detected in the absence of phonon–phonon interactions with allowance for only elastic WNP scattering. Thus, this method can be informative for studying two-level systems (TLSs), spin interactions, and local vibrational states in the temperature range $T < 4$ K [20, 21].

As was shown in [22], which was one of the first theoretical works dealing with the phonon transport in amorphous media in terms of the general soft potential model (which also includes a TLS model in the limiting case), the temperature dependences of the signal-peak delay time and the diffusion coefficient are $t_m(T) \propto T^{-n}$ and $D(T) \propto T^{-n}$ ($n > 4$), respectively, under the experimental conditions described above in the temperature range preceding the thermal conductivity plateau, and these dependences were observed in glasses of various compositions [21]. A "hot" spot was shown to form in fused silica at the contact with an injector [21]. According to the estimate from review [23], the spot size along WNP propagation is 100 μm at $T = 4$ K. However, we [20] did support this finding when analyzing the transport characteristics of WNP in a strongly imperfect yttrium-stabilized zirconia single crystal with TLS, which were caused by the presence of vacancies in the anion sublattice. The broad boson peak in the temperature dependence c/T^3 was shifted toward high temperatures, which is typical of single crystals. Therefore, we concluded that the assumption about glassy nature of the detected kinetic characteristics was not confirmed in single crystals.

The existence of low-energy states at the same temperatures manifests itself in specific heat. To theoretically describe the experimental temperature dependences of the specific heat $c(T)$ of the materials under study, we have to take into account the contribution of magnetic centers to specific heat, which is usually calculated in a TLS model, along with the traditional lattice contributions (Debye contribution, Einstein modes). In this case, an analysis of the temperature dependences of the kinetic characteristics of phonons in combination with the measurement of the temperature dependences of specific heat makes it possible to study the relation between the kinetic and thermophysical characteristics of REAG solid solutions [12]. In addition, the propagation of a short heat pulse is a fundamentally nonstationary process. Therefore, we can analyze the influence of the spatial inhomogeneity related to the coordinate dependence of the state of low-energy TLSs on the transport characteristics of WNP when equilibrium (thermalization) is reached in the WNP–TLS system.

3. RESULTS AND DISCUSSION

We studied the temperature dependences of specific heat $c(T)$ and the transport characteristics of phonons in Er-containing single crystals of the solid solutions $Y_{3-x}Er_xAl_5O_{12}$ (x = 0.2, 0.6, 1.1, 3), $Er_xTm_{3-x}Al_5O_{12}$ (x = 0, 1, 2, 3), and $Er_2HoAl_5O_{12}$.

Our preliminary investigations [12] showed a significant effect of low-energy excitations on the $c(T)$ temperature dependences and an anomalous character of the temperature dependences of the transport characteristics of phonons.

The energy of the lowest level of the $^4I_{15/2}$ multiplet in YAG:Er^{3+} is known to be 30–40 K at various Er concentrations, which is much higher than the thermal-frequency phonon energy at liquid-helium temperatures. However, the Kramers character of the Er^{3+} ion implies the possibility of removing the degeneracy of the ground state in a zero applied magnetic field due to the interaction of the magnetic moments of neighboring Er^{3+} ions [7, 12]. Along with Ho^{3+}, this character determines an anomalous character the phonon transport in the $Er_2HoAl_5O_{12}$ single crystal at $T < 4$ K.

The $c(T)$ temperature dependences in single crystals of the $Y_{3-x}Er_xAl_5O_{12}$ ($x = 0.6$, 1.1, 3) solid solutions in the temperature range 1.9–220 K were measured in [24]. The excitation energies were determined by standard fitting with allowance for The Debye contribution and Einstein modes.

As is seen in Fig. 1, the $c(T)$ dependence in the YAG:Er ($x = 1.1$) sample in the temperature range $T <$ 4 K is satisfactorily described by the energy of the lowest Stark level ($\Delta_1 = 34$ K) and the existence of low-energy TLS ($\Delta = 1.3$ K).

Table 1 gives the results of estimating the splitting energy of the ground state in Er-containing REAG solid solutions from [24]. As the Er concentration increases, Δ increases to $\Delta = 1.3$ K at a solid solution concentration of about 33% and then decreases to about 1 K.

Figure 2 shows the WNP pulses $S(t)$ detected in $Y_{2.8}Lu_{0.2}Al_5O_{12}$, $Y_{2.8}Er_{0.2}Al_5O_{12}$, and $Y_{1.5}Er_{1.5}Al_5O_{12}$ samples by a bolometer in the diffusion mode at various thermostat temperatures. The first two samples had the same geometry and length ($L = 0.68$ cm).

In the absence of a phonon–phonon interaction in the YAG:$Lu_{0.2}$ sample, the signal position and shape in Fig. 2a give information only on elastic phonon scattering, which is caused by the difference between the masses of the Y^{3+} ion and the nonmagnetic rare-earth Lu^{3+} ion.

The increase in the time of detecting the signal maximum in the sample where Er^{3+} substitutes for Lu^{3+} at the same degree of doping (Fig. 2b), the significant increase in the signal delay, and the change in the sign of derivative dt_m/dT at a higher Er^{3+} concentration

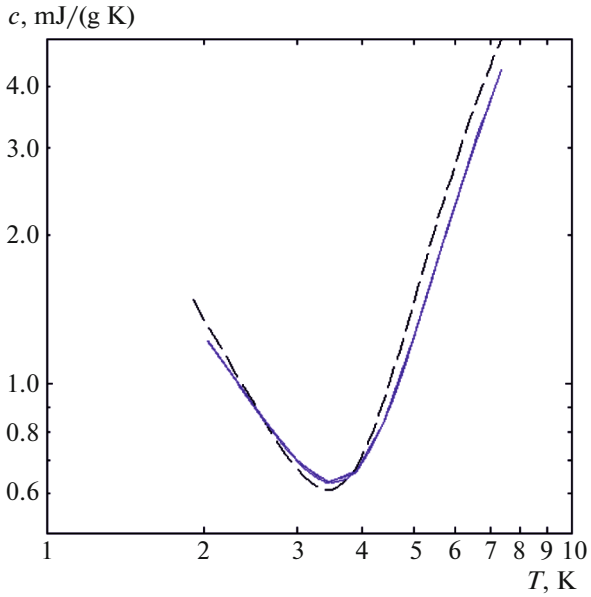

Fig. 1. (Color online) Experimental (solid curve) and calculated (dashed curve) temperature dependences of the specific heat of $Y_{1.9}Er_{1.1}Al_5O_{12}$.

in a sample (Fig. 2c) are associated with the low-energy excitations described above, which determine the $c(T)$ dependence in the temperature range under study.

When analyzing the phonon propagation in a medium with low-energy excitations by the TLS model, we can relate the long signal delay times in Figs. 2b and 2c as compared to the case in Fig. 2a to the sequence of phonon trapping and reemission by a TLS that is caused by the Kramers nature of the Er^{3+} ion during intense elastic (Rayleigh) thermal-frequency phonon scattering because of the difference between the masses of the Y^{3+} and Re^{3+} ions at the c lattice sites in the garnet.

The fact that the times of the maximum and the signal shapes in Figs. 2a and 2b coincide can be used to determine the mean free path and time of phonons with respect to scattering (trapping) by TLS in the $Y_{2.8}Lu_{0.2}Al_5O_{12}$ sample at a given temperature using the following expression from the general diffusion theory (which is analogous to Eq. (2)):

$$l_R = \sqrt{D_0\tau_R} \geq L, \tag{3}$$

where l_R and τ_R are the mean free path of WNP and the time with respect to phonon trapping by TLS, respec-

Table 1

	$Y_{2.4}Er_{0.6}Al_5O_{12}$	$Y_{1.9}Er_{1.1}Al_5O_{12}$	$Er_3Al_5O_{12}$	$ErTm_2Al_5O_{12}$	$Er_2TmAl_5O_{12}$	$Er_2HoAl_5O_{12}$
Δ, K	0.6	1.3	1.1	0.7	1.0	1.0

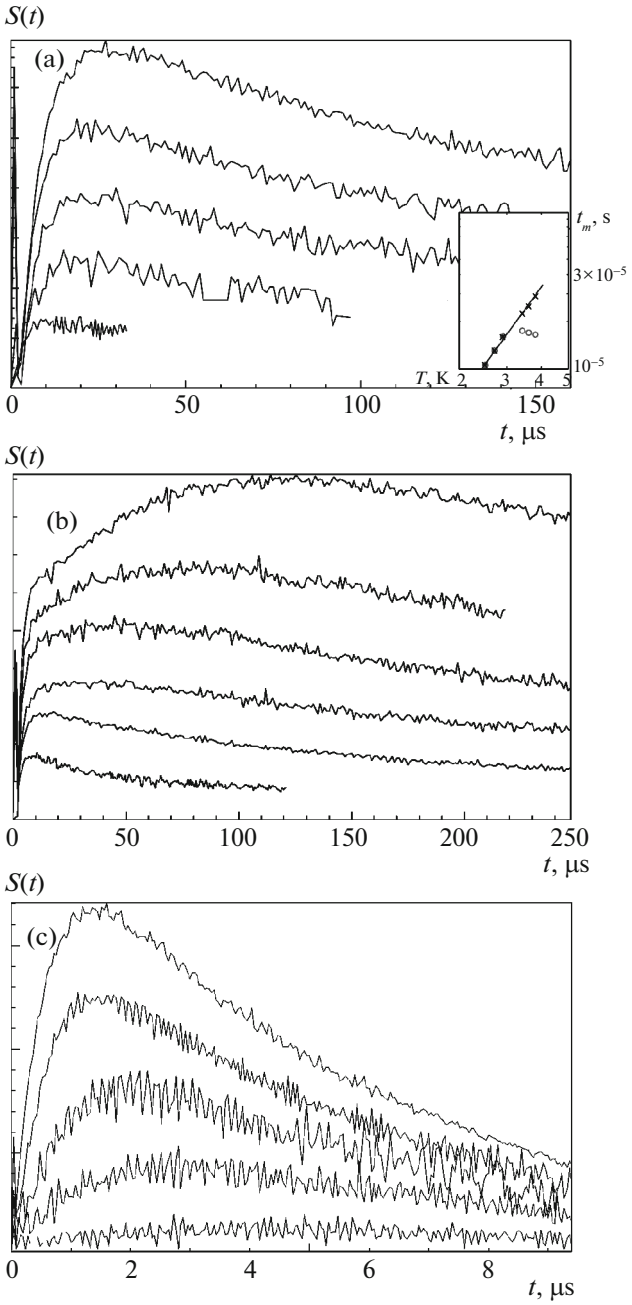

Fig. 2. WNP propagation in samples: (a) $Y_{2.8}Lu_{0.2}Al_5O_{12}$ at $T = 3.83$, 3.43, 2.91, 2.53, and 2.3 (from top to bottom); (inset) temperature dependences of the time of (×) signal maximum in $Y_{2.8}Lu_{0.2}Al_5O_{12}$ and first maximum in (○) $Y_{2.8}Er_{0.2}Al_5O_{12}$ ($L = 0.68$ cm); (b) $Y_{2.8}Er_{0.2}Al_5O_{12}$ at $T = 3.77$, 3.38, 3.12, 2.91, 2.54, and 2.2 K (from top to bottom); (c) $Y_{1.5}Er_{1.5}Al_5O_{12}$ ($L = 0.60$ cm) at $T = 3.87$, 3.5, 2.95, 2.57, and 2.24 K (from top to bottom).

tively, and $L = 0.68$ cm is the sample length. D_0 can be found using Eq. (1) accurate to the geometric factor from the time of arrival of the signal maximum in the $Y_{2.8}Lu_{0.2}Al_5O_{12}$ sample at $T = 2.91$ K ($D_0 = 10^4$ cm^2/s); here, we have $\tau_R \sim 10^{-5}$ s.

Thus, the presence of the Er^{3+} ion in YAG leads to the formation of low-energy TLSs, which retard the transport of thermal-frequency phonons at liquid-helium temperatures.

We now consider the temperature dependences $t_m(T)$ in samples of various lengths in the WNP propagation direction for the composition $Y_{3-x}Er_xAl_5O_{12}$ ($x = 1.1$); they reflect the state of the WNP–TLS system. As follows from Figs. 2b and 2c, the signal shape and the signal propagation time strongly depend on the existence of the paramagnetic Er^{3+} ion in the system. This phenomenon was theoretically explained in [25], where one-dimensional heat pulse propagation was considered in a system with inelastic phonon scattering centers (trapping centers) using the TLS model. In the general case, the following two WNP fluxes were shown to appear: a fast flux formed by the phonons that had no time to interact with trapping centers (according to Eq. (1), the flux propagation time is determined by diffusion coefficient D_0, which depends only on the elastic phonon scattering by defects), and a slow flux, the phonons of which were trapped and reemitted by TLS during propagation. The slow flux propagation time is $t_m = L^2/2D$, where D is the effective diffusion coefficient of WNPs.

The contribution of each flux to the total flux is determined by the ratio of the pulse propagation time in the absence of trapping centers (t_{m0}) and the phonon–TLS interaction time (τ_R). At $k = t_{m0}/\tau_R \ll 1$ (weak or absent interaction), the position of the signal peak only give information on elastic phonon scattering (see Fig. 2a). In the reverse situation ($k \gg 1$), WNP propagation is retarded for most phonons (interaction with TLS), and the time of arrival of a signal peak at a bolometer is determined by slow processes (Fig. 2c). If k is about unity, the bolometer can detect two peaks, which can be resolved at $D \ll D_0$ (see Fig. 2b). At low temperatures, such a situation can appear in the presence of TLSs energy parameter Δ of which falls in the temperature (energy) range of WNPs.

According to Eq. (1), t_{m0} from the expression for k depends on the sample length in the heat pulse propagation direction, which was regularly changed under experimental conditions. Figure 3, which was plotted using the data from [14], illustrates the dependence of t_{m0} on concentration x and type of doping impurity Re^{3+} in $Y_{3-x}Re_xAl_5O_{12}$ samples of various lengths over the entire x range at $T = 3.4$ K.

As was shown in [25], the $t_m(T)$ temperature dependence at $k \gg 1$ is related to the specific heat of the system ($c = c_{ph} + Nc_{tls}$) by the expression

$$t_m(N,T) = t_{m0}(T)\left(1 + \frac{Nc_{tls}}{c_{ph}}\right) \propto \frac{t_{m0}(T)Nc_{tls}}{c_{ph}}, \qquad (4)$$

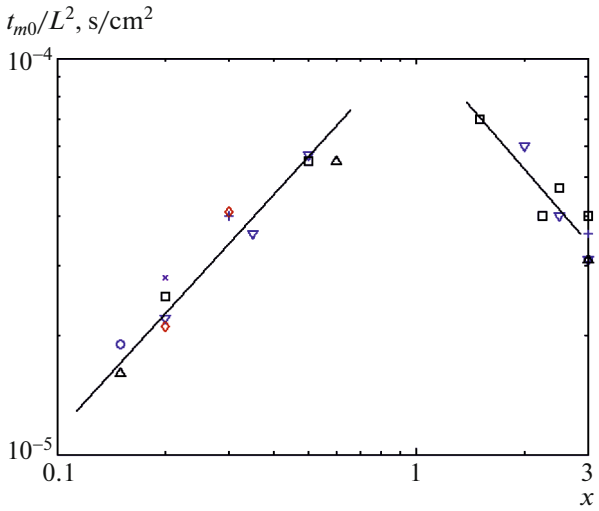

Fig. 3. (Color online) Characteristic t_{m0} of elastic (Rayleigh) WNP scattering normalized by the length squared vs. the concentration and type of doping impurity Re^{3+} in $Y_{3-x}Re_xAl_5O_{12}$ samples at a thermostat temperature $T = 3.4$ K (Re is a rare-earth element): Re = (△) Yb, (□) Dy, (○) Er, (◇) Tb, (▽) Lu, (+) Tm, and (×) Ho.

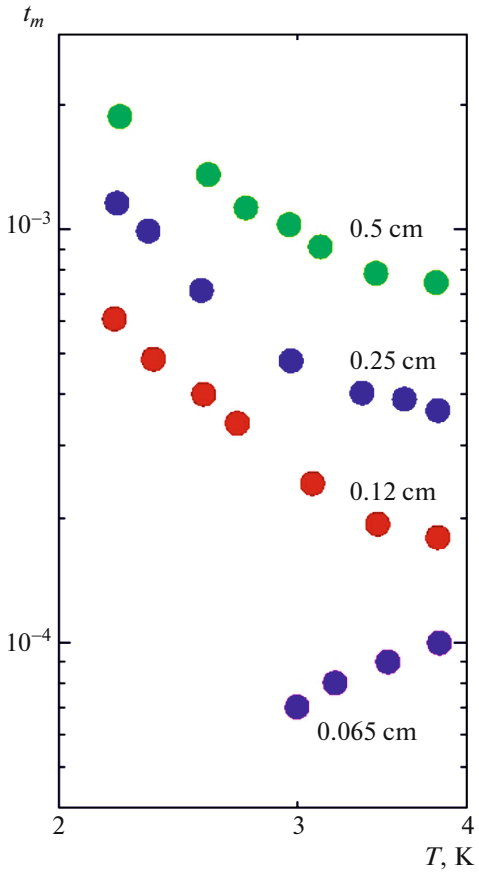

Fig. 4. (Color online) Temperature dependences of the time of arrival of the WNP signal maximum at a bolometer in $ErY_2Al_5O_{12}$ samples of various lengths.

where $c_{tls}(T)$ and N are the specific heat and the number of TLSs, respectively; c_{ph} is the specific heat of phonons, and the last approximate equality is valid when the condition $Nc_{tls} \gg c_{ph}$ is met. Equation (4) reflects the relation between the independent experiments on determining $t_m(T)$ and $c(T)$. Here, we have $t_m(T) > t_{m0}$.

Figure 4 depicts the temperature dependences of the time of arrival of a WNP signal peak at the bolometer for $Er_1Y_2Al_5O_{12}$ samples of various lengths. Here, slow processes are predominant, which is indicated by the sign of the derivative and an anomalous (not diffusional $t_{m0} \propto L^2$) dependence of the time of arrival of a signal peak on the sample length ($t_m \propto L$). This length dependence directly follows from Eq. (4), since the number of TLSs is the same for all samples: $N = SLn_{tls}$, where $S = 1$ cm^2 is the sample area and n_{tls} is the number of TLSs per unit volume.

Figure 5 shows $t_m(T)/L$ measured for three samples, and these data are seen to be near curve *1*. Curve *2* is the $t_m(T)$ dependence for a sample 0.065 cm long, in which the TLS trapping length is comparable with the sample length.

The possibility of equals sign in the relation between the left-hand (kinetic) and the right-hand (thermodynamic) sides of Eq. (5), which was derived from Eq. (4) at $n_{tls}c_{tls} \gg c_{ph}$,

$$\frac{t_m(T)}{Lt_{m0}} \approx \frac{n_{tls}c_{tls}}{c_{ph}}, \qquad (5)$$

makes it possible to determine the sample length and time $t_m(T)$ at which thermalization is possible in the WNP–TLS system. The estimation was performed as follows: the values of $c(T)$ were taken from the specific heat data and the calculated Debye temperature for $Y_{3-x}Re_xAl_5O_{12}$ ($x = 1.1$), and $T_D = 731$ K was taken from [7]. As follows from [26], T_D for rare-earth garnets is the same (molar masses are almost the same). Table 2 gives $t_{m0}(L, T)$, $t_m(L, T)$, $n_{tls}c_{tls}$, and c_{ph} for three temperatures from the range under study for each sample.

The calculation of the ratio of the left-hand side to the right-hand side of Eq. (5) at each temperature for samples of length $L = 0.12$, 0.25, and 0.5 cm demonstrates that this ratio is close to unity only for a sufficiently long sample ($L > 0.25$ cm) at a delay temperature $t_m(T, L) \geq 10^{-3}$ s. The thermalization conditions are improved when the thermostat temperature increases. This result does not contradict the estimates from [27], where the possibility of thermalization was discussed for the phonon–TLS system due to effective TLS anharmonicity in the absence of a phonon–phonon interaction.

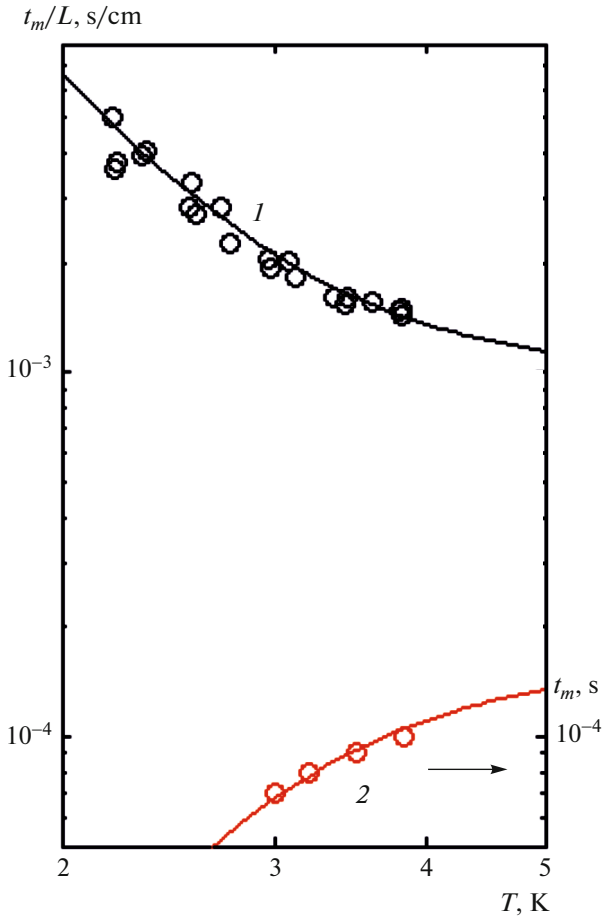

Fig. 5. (Color online) (*1*) Experimental results of measuring $t_m(T)/L$ for three samples and (*2*) dependence $t_m(T)$ for a sample 0.065 cm long.

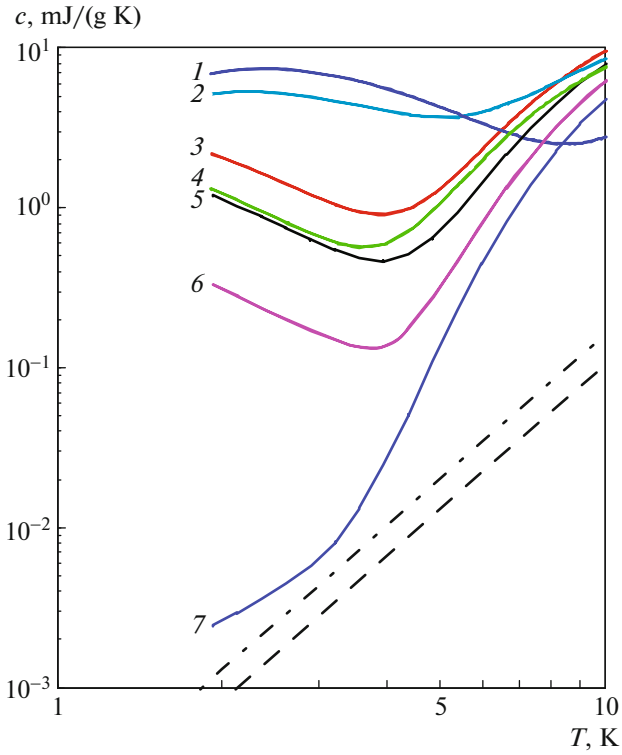

Fig. 6. (Color online) $c(T)$ dependences in the following REAG samples: (*1*) $Y_{1.5}Ho_{1.5}Al_5O_{12}$, (*2*) $Er_2HoAl_5O_{12}$, (*3*) $Er_3Al_5O_{12}$, (*4*) $Y_2ErAl_5O_{12}$, (*5*) $Er_2TmAl_5O_{12}$, (*6*) $ErTm_2Al_5O_{12}$, and (*7*) $Tm_3Al_5O_{12}$. Calculated $c_{ph}(T)$ dependence for (dot-and-dash line) $Y_2Er_1Al_5O_{12}$ and (dashed line) $Er_3Al_5O_{12}$.

Figure 7 shows the time dependences of a WNP signal at various thermostat temperatures in mixed REAG samples, namely, $Er_2TmAl_5O_{12}$ (L = 3.9 mm) and $ErTm_2Al_5O_{12}$ (L = 3.9 mm). All REAG samples are characterized by a large molecular mass, a very small mass defect at substitution sites, and (hence) a negligibly small difference in WNP elastic scattering. Therefore, the specific features of scattering in the samples in the temperature range under study are mainly caused by the existence of low-energy TLSs.

The quasi-ballistic character of WNP propagation in short samples (insets to Figs. 7a, 7b) allows us to estimate the free path length and the time with respect to TLS trapping by Eq. (3). For almost all mixed

Table 2

L, cm		T = 2.4 K	T = 3.0 K	T = 2.4 K
0.012	t_m, s	2×10^{-4}	2.1×10^{-4}	4×10^{-4}
	t_{m0}, s	1.44×10^{-6}	8.6×10^{-7}	3.6×10^{-7}
0.25	t_m, s	4×10^{-4}	5×10^{-4}	8×10^{-4}
	t_{m0}, s	6.25×10^{-6}	3.75×10^{-6}	1.56×10^{-6}
0.5	t_m, s	8×10^{-4}	9×10^{-4}	1.65×10^{-3}
	t_{m0}, s	2.5×10^{-5}	1.5×10^{-5}	6.2×10^{-6}
	$n_{tls}c_{tls}$, μJ/(mg K)	6×10^{-1}	6.5×10^{-1}	1
	c_{ph}, μJ/(mg K)	6×10^{-3}	4×10^{-3}	2×10^{-4}

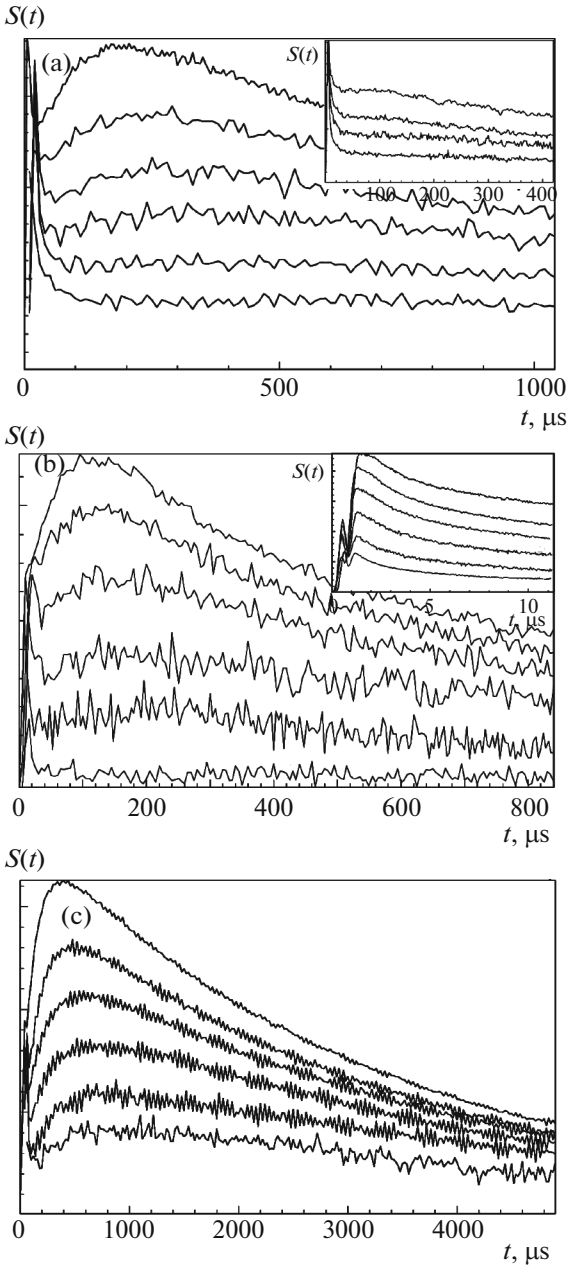

Fig. 7. Temperature dependences of the time of arrival of the WNP signal maximum: (a) $Er_2TmAl_5O_{12}$ (L = 3.9 mm), (b) $ErTm_2Al_5O_{12}$ (L = 3.9 mm), and (c) $Er_2HoAl_5O_{12}$ (L = 0.42 mm). T = 3.88, 3.63, 3.41, 3.16, 2.90, and 2.51 K (from top to bottom). (insets) Signals of these samples at a smaller length (L = 1.2 mm).

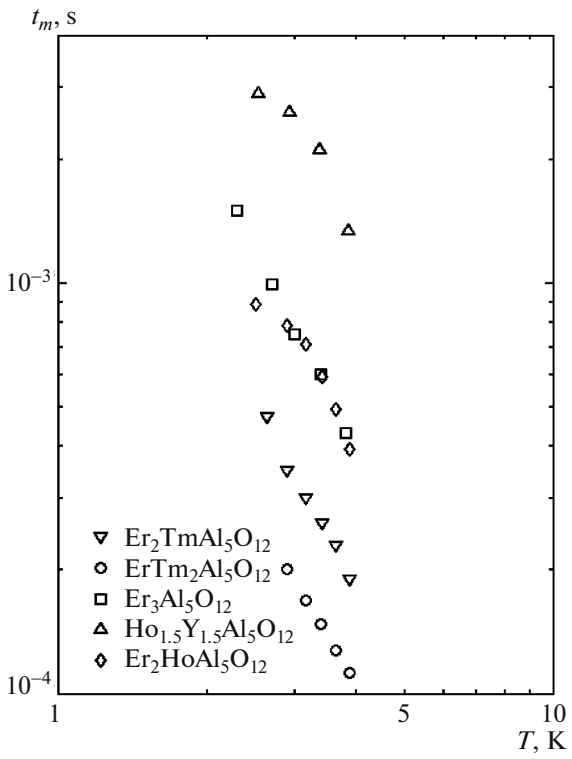

Fig. 8. Experimental $t_m(T)$ dependences in samples $ErTm_2Al_5O_{12}$, $Er_2TmAl_5O_{12}$, $Er_3Al_5O_{12}$, $Er_2HoAl_5O_{12}$, and $Y_{1.5}Ho_{1.5}Al_5O_{12}$ from [12].

REAGs, we have $D_0 \approx 10^4$ cm^2/s at $T = 3$ K. The estimation at $T = 3$ K demonstrates that $\tau_R \geq 10^{-6}$ s for $Er_2TmAl_5O_{12}$, which does not contradict the data obtained for the $Y_{2.8}Er_{0.2}Al_5O_{12}$ sample on the assumption that $\tau_R \propto 1/N$. (According to [27], the TLS reemission time at $T = 3$ K is 10^{-7} s.)

The intense WNP scattering in the short $Er_2HoAl_5O_{12}$ sample is related to the presence of additional low-energy levels of the Ho^{3+} ion (Δ = 5.8 K), which are caused by a decrease in the symmetry of the local crystal field (Fig. 7c) [8]. At $T = 3$ K, we have $\tau_R \geq 10^{-8}$ s.

Figure 8 shows the experimental $t_m(T)$ dependences of the $ErTm_2Al_5O_{12}$, $Er_2TmAl_5O_{12}$, $Er_3Al_5O_{12}$, and $Er_2HoAl_5O_{12}$ samples. The ratio of the left-hand side to the right-hand side of Eq. (5) is close to unity, when thermalization can occur in the WNP–TLS system, only in the $Y_{1.5}Ho_{1.5}Al_5O_{12}$, $Er_3Al_5O_{12}$, and $Er_2TmAl_5O_{12}$ samples.

Thus, we studied the WNP transport in REAG at liquid-helium temperatures in the presence of low-energy excitations and estimated the characteristic phonon lifetimes upon scattering by TLS. We also determined thermalization conditions in the WNP–TLS system in the absence of a phonon–phonon interaction under conditions of a nonstationary process and the spatial inhomogeneity caused by the coordinate dependence of the state of TLS.

The temperature dependences of the specific heat $c(T)$ of Er-containing REAG samples were analyzed on a PPMS-9 + Ever-Cool-II (Quantum Design) device with an embedded option. The measurements

were carried out in the temperature range 1.9–220 K. Solid solution $Y_{3-x}Er_xAl_5O_{12}$ ($x = 0.2, 0.6, 1.1, 3$) single crystals were grown from a melt by horizontal directional solidification in a molybdenum container.

ACKNOWLEDGMENTS

We thank A.A. Kaminskii for the possibility of studying the mixed REAG samples.

This work was supported in part by the Presidium of the Ural Branch, Russian Academy of Sciences (project no. 18-2-2-12, AAAA-A16-116021010082-8) and the Russian Foundation for Basic Research (project nos. 16-07-00592, 16-07-00181, 18-07-00191).

REFERENCES

1. W. Koechner, *Solid State Laser Engineering* (Springer, Berlin, 2006).
2. A. A. Kaminskii, *Laser Crystals* (Springer, New York, 1981).
3. Glen A. Slack and D. W. Oliver, Phys. Rev. B **4**, 592 (1971).
4. V. L. Gurevich, *Transport in Phonon Systems* (North-Holland, Amsterdam, 1986).
5. S. N. Ivanov, IEEE Trans. Ultrason. Ferroelectr. Freq. Control **39**, 653 (1992).
6. A. A. Kaminskii, A. V. Taranov, E. N. Khazanov, and M. Sh. Akchurin, Quantum Electron. **42**, 880 (2012).
7. A. Kushino, Y. Aoki, N. Y. Yamasaki, T. Namiki, Y. Ishisaki, T. D. Matsuda, T. Ohashi, K. Mitsuda, and T. Yazawa, J. Appl. Phys. **90**, 5812 (2001).
8. S. Nagata, H. Sasaki, K. Suzuki, J. Kiuchi, and N. Wada, J. Phys. Chem. Sol. **62**, 1123 (2001).
9. K. Kamazawa, D. Louca, R. Morinaga, T. J. Sato, Q. Huang, J. R. D. Copley, and Y. Qiu, Phys. Rev. B **78**, 064412 (2008).
10. E. V. Shevchenko, E. V. Charnaya, E. N. Khazanov, A. V. Taranov, and A. S. Bugaev, Phys. Solid State **59**, 733 (2017).
11. E. V. Shevchenko, E. V. Charnaya, M. K. Lee, L. J. Chang, E. N. Khazanov, A. V. Taranov, and A. S. Bugaev, Phys. Lett. A **381**, 330 (2017).
12. E. N. Khazanov, A. V. Taranov, E. V. Shevchenko, and E. V. Charnaya, J. Exp. Theor. Phys. **121**, 48 (2015).
13. I. B. Levinson, JETP Lett. **27**, 181 (1978).
14. S. N. Ivanov, E. N. Khazanov, T. Paszkiewicz, A. V. Taranov, and M. Wilczyński, Z. Phys. B **99**, 535 (1996).
15. R. J. Gutfeld and A. H. Nethercot, Jr., Phys. Rev. Lett. **12**, 641 (1964).
16. D. V. Kazakovtsev and Y. B. Levinson, Phys. Status Solidi B **136**, 425 (1986).
17. Y. K. Yogurtsu, A. J. Miller, and G. A. Sanders, Phys. C **13**, 6585 (1980).
18. S. N. Ivanov, A. V. Taranov, and E. N. Khazanov, Sov. Phys. JETP **72**, 731 (1991).
19. S. N. Ivanov, E. N. Khazanov, and A. V. Taranov, Sov. Phys. Solid State **29**, 385 (1987).
20. E. I. Salamatov, A. V. Taranov, E. N. Khazanov, E. V. Charnaya, and E. V. Shevchenko, J. Exp. Theor. Phys. **125**, 768 (2017).
21. E. I. Salamatov, A. V. Taranov, and E. N. Khazanov, J. Exp. Theor. Phys. **121**, 267 (2015).
22. V. I. Kozub, A. M. Rudin, and H. R. Schober, Phys. Rev. B **50**, 6032 (1994).
23. V. I. Kozub and A. M. Rudin, Phys. Solid State **38**, 189 (1996).
24. E. V. Shevchenko, E. V. Charnaya, E. N. Khazanov, A. V. Taranov, and A. S. Bugaev, J. Alloys Compd. **717**, 183 (2017).
25. E. I. Salamatov, Phys. Solid State **44**, 978 (2002).
26. M. G. Beghi, C. E. Bottani, and V. Russo, J. Appl. Phys. **87**, 1769 (2000).
27. I. B. Levinson, JETP Lett. **37**, 190 (1983).

Translated by K. Shakhlevich